Adaptive Beat Suppression Strategy Based on Voltage Angle Harmonics Regulation for Electrolytic Capacitorless PMSM Drives

Tianqi Zhang, Dawei Ding, *Member, IEEE*, Gaolin Wang, *Senior Member, IEEE*, Yihua Hu, *Senior Member, IEEE*, Guoqiang Zhang, *Senior Member, IEEE*, and Dianguo Xu, *Fellow, IEEE*

***Abstract*—The beat phenomenon in electrolytic capacitorless permanent magnet synchronous motor (PMSM) drives is serious within field-weakening (FW) region. This article proposes an adaptive beat suppression strategy through regulating the voltage angle harmonics. By dividing the admittance in FW region into voltage sampling time-delay admittance and FW characteristic admittance, the relationship between beat envelope and the admittances is quantitatively analyzed. It is revealed that the conventional method can only reduce the influence of voltage sampling time-delay admittance. The proposed strategy constructs a closed-loop harmonic control of the dc-link voltage and the voltage angle to minimize the amplitude of beat envelope. By reshaping the impedance relationships between dc-link voltage and motor currents at inherent frequency, the FW characteristic admittance is reduced and the beat phenomenon in this region is suppressed effectively. Based on the reshaped impedance model, the control parameters are adaptively regulated with the motor speed and *dq*-axis currents. Experimental results show the effectiveness of the proposed method in a PMSM system with small dc-link capacitors.**

***Index Terms*—Beat suppression, field-weakening (FW), permanent magnet synchronous motor (PMSM), small dc-link capacitor, voltage angle.**

I. Introduction

PERMANENT magnet synchronous motor (PMSM) has the advantages of simple structure, high power density, and high efficiency, which is widely used in electric vehicles, heating, ventilation, and air conditioning (HVAC) [1], [2], [3], [4], [5]. The electrolytic capacitorless PMSM drives replace the traditional electrolytic capacitors with film capacitors, which have the advantages of high-temperature resistance, smaller size, low cost, and improved power quality in grid-side. This configuration makes them especially suitable for HVAC applications [6], [7], [8]. However, the reduction of the dc-link capacitance will amplify the harmonics of the dc-link voltage, which causes serious harmonic problems.

In order to solve the inherent harmonics problems, which are directly related to the dc-link frequency, some effective methods are proposed. In [9], a grid current harmonic suppression method for parallel compensator on the dc-link was proposed, which can adjust the harmonic power to suppress the harmonics at middle and high frequencies. The *LC* resonance caused by the dc-link inductor and capacitor aggravates the harmonics between the grid and motor sides, and the negative impedance characteristic of the tight controlled motor further exacerbates the problem [10], [11]. In [12], the resonance was suppressed by compensating for the dc-link voltage used for modulation, which can effectively reduce the distortions of the grid current and the dc-link voltage. In [10], the impedance of the intrinsic harmonics near the resonance was designed to accurately control the grid current harmonics and reduce the interference on the motor side. Based on the concept of frequency mapping, the harmonics of grid current at high frequencies can be reduced by reshaping the impedance at lower frequencies [13].

In addition to the aforementioned inherent harmonics, the beat phenomenon caused by the harmonics coupling, is a gap of electrolytic capacitorless motor drives in industrial application [14]. The sampling error of the dc-link voltage in the modulation will lead to the output voltage error, and the dc-link voltage harmonics will be reflected in the motor voltage, resulting in the motor current beat phenomenon [15]. One of the mainstream methods to solve the beat phenomenon is adding additional hardware. The easy hardware method is to connect *LC* resonant filters in parallel on the dc-link to absorb the pulsating power [16]. In [17], a new boost-based active power decoupling circuit was proposed to suppress voltage fluctuations, and the energy flow in the boost and power decoupling links were complementarily controlled to effectively reduce harmonics of voltage and motor current. In [18], the estimated voltage harmonics were compensated into the windings by an additional inverter to reduce the current harmonics. The method of changing the topology of the drive is

Received 17 May 2025; revised 27 July 2025; accepted 22 August 2025. Date of publication 29 August 2025; date of current version 22 October 2025. This work was supported in part by the Research Fund for the National Natural Science Foundation of China under Grant 52207042, Grant 52125701, and Grant 52421004, in part by the Young Elite Scientists Sponsorship Program by CAST under Grant 2023QNRC001, in part by the Fellowship from the China Postdoctoral Science Foundation under Grant 2025T181153, and in part by New Era Longjiang Excellent Master's and Doctoral Thesis Funding Project under Grant LJYXL2022-048. Recommended for publication by Associate Editor M. Hartmann. *(Corresponding author: Dawei Ding.)*

Tianqi Zhang, Dawei Ding, Gaolin Wang, Guoqiang Zhang, and Dianguo Xu are with the School of Electrical Engineering and Automation, Harbin Institute of Technology, Harbin 150001, China (e-mail: 23s106168@stu.hit.edu.cn; dingdawei@hit.edu.cn; wgl818@hit.edu.cn; zhgq@hit.edu.cn; xudiang@hit.edu.cn).

Yihua Hu is with the Department of Engineering, King's College London, WC2R2LS London, U.K. (e-mail: yihua.hu@kcl.ac.uk).

Color versions of one or more figures in this article are available at https://doi.org/10.1109/TPEL.2025.3604231.

Digital Object Identifier 10.1109/TPEL.2025.3604231

stable and robust. However, the additional hardware increases the cost and size of the system. Hence, the software algorithms of beat suppression are more preferred in HVAC systems.

One of the software solutions to suppress the beat phenomenon is to reduce the sampling and calculation delay of the dc-link voltage, and reduce the output error of the modulation. In [19], a dc-link voltage repeat observer was proposed to compensate for the calculation of the pulse width modulation, which can predict the average of dc-link voltage of the next switching cycle to reduce the beat phenomenon in the track traction system. Similarly, the dc-link voltage can be reconstructed by delaying the harmonics of the dc-link voltage to reduce sampling and update errors [8], [20], [21]. However, the beat phenomenon in the field-weakening (FW) region is not completely caused by the sampling delay of voltage, so the beat phenomenon suppression by predicting the dc-link voltage has limited effect.

The beat suppression can also be achieved by changing the impedance characteristics of the system. The low-frequency harmonics of the output current caused by dc-link voltage fluctuations and dead time can be reduced by connecting virtual resistors and inductors in series on the load side [22]. In [23], a beat suppression method based on impedance reshaping was proposed, which realized the simultaneous suppression of motor current and grid current harmonics. In [24], the output current ripple was suppressed by adding a power current control loop between the two closed loops. Meanwhile, the harmonic at the frequency of dc-link voltage fluctuation can be added to the power current reference to extend to the smaller dc-link capacitance drive system. The periodic power harmonics can be also regulated by a power balance resonant controller, which suppresses the beat phenomenon of grid current caused by the interaction of the dc-link voltage fluctuation and load fluctuation [25]. The above methods can effectively suppress the beat phenomenon in the constant torque region. However, the change of impedance characteristics during the FW control has not been considered, resulting in a limited effect on beat suppression.

In this article, an adaptive beat suppression strategy based on voltage angle harmonics regulation is proposed to improve the performance in the FW region. By establishing the transfer functions between the motor currents and the dc-link voltage, the impact of voltage sampling time-delay admittance (VST-A) and FW characteristic admittance (FWC-A) on the motor current beat phenomenon is firstly clarified. Furthermore, the limitations of existing schemes in controlling FWC-A are analyzed from an impedance perspective. The impedance relationship with the minimum beat envelope is analyzed, which is used to establish a closed-loop control of voltage angle harmonic. Relying on the impedance relationship, the desired voltage angle harmonics can be obtained from the dc-link voltage harmonics. Furthermore, the parameters of harmonic synthesis can be self-tuned based on motor speed and *dq*-axis currents. The proposed method can effectively reduce FWC-A, thereby having a better beat suppression effect in the FW region than the conventional method. And the method has satisfactory adaptability to the operating conditions and parameters of the motor. The proposed method is experimentally verified on a PMSM system with small dc-link capacitors.

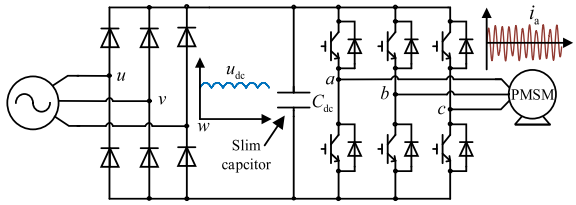

Fig. 1. Topology of PMSM drive with small DC-link capacitors.

II. Analysis of Beat Phenomenon Under FW Control of Electrolytic Capacitorless Drive

A. Beat Phenomenon in Motor Currents

The topology of the three-phase motor drive with small dc-link capacitors is shown in Fig. 1. The rectified voltage u_{grec} can be expressed as

$$\begin{aligned} u_{\mathrm{grec}} &= U_{\mathrm{grec0}} + \sum_{k=1}^{\infty} U_{\mathrm{greck}} \sin(6k\omega_g t + \varphi_{\mathrm{greck}}) \\ &= \frac{3\sqrt{2}}{\pi} U_{\mathrm{g}} + \sum_{k=1}^{\infty} -\frac{6\sqrt{2} U_{\mathrm{g}} \cos(k\pi)}{\pi(36k^2-1)} \cos(6k\omega_{\mathrm{g}} t) \end{aligned} \tag{1}$$

where U_{grec0}, U_{greck}, and φ_{greck} are the average, the amplitude, and the phase of the kth harmonics of the rectified voltage, respectively. U_{g} and ω_{g} are the root mean square value of the input line-to-line voltage and the grid frequency, respectively.

According to Fig. 1, the transfer function between u_{grec} and the dc-link voltage u_{dc} can be expressed as

$$\frac{\Delta u_{\mathrm{dc}}}{\Delta u_{\mathrm{grec}}} = \frac{1}{1 + (L_{\mathrm{eq}} s + R_{\mathrm{g}}) \left[\boldsymbol{Y}_{\mathrm{m}}(s) + C_{\mathrm{dc}} s \right]} \tag{2}$$

where R_{g} is the equivalent line resistance, C_{dc} is the dc-link capacitance, L_{eq} is the equivalent inductance, and $\boldsymbol{Y}_{\mathrm{m}}$ is the input admittance of inverter.

The amplitude of the dc-link voltage fluctuation can be quantitatively analyzed through (2). After the capacitance is greatly reduced, its energy storage capacity decreases, and the dc-link voltage u_{dc} has a periodic fluctuation of 6k times the frequency of the grid, which can be expressed as

$$u_{\mathrm{dc}} = U_{\mathrm{dc0}} + \sum_{k=1}^{\infty} U_{\mathrm{dck}} \sin(6k\omega_{\mathrm{g}} t + \varphi_{\mathrm{k}}) \tag{3}$$

where U_{dc0} is the average of the dc-link voltage. U_{dck} and φ_{k} are the amplitude and phase of the $6k\omega_{\mathrm{g}}$ harmonic of the dc-link voltage, respectively.

Affected by the dc-link voltage sampling update and modulation, there are also harmonics at the same frequency as the dc-link voltage in the amplitude of the motor voltage vector, and the harmonics at the same frequency will also be reflected in the *dq*-axis currents $i_{\mathrm{d,q}}$

$$\begin{cases} i_{\mathrm{d}} = I_{\mathrm{d0}} + \sum\limits_{k=1}^{\infty} I_{\mathrm{dk}} \sin(6k\omega_{\mathrm{g}} t + \varphi_{\mathrm{dk}}) \\ i_{\mathrm{q}} = I_{\mathrm{q0}} + \sum\limits_{k=1}^{\infty} I_{\mathrm{qk}} \sin(6k\omega_{\mathrm{g}} t + \varphi_{\mathrm{qk}}) \end{cases} \tag{4}$$

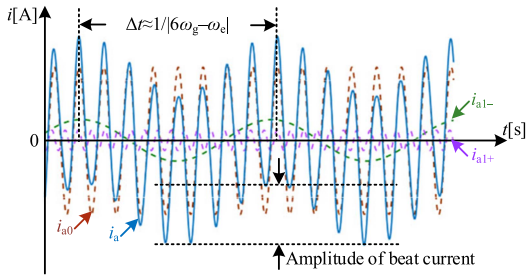

Fig. 2. Schematic diagram of beat phenomenon due to the interaction between fundamental and harmonic currents.

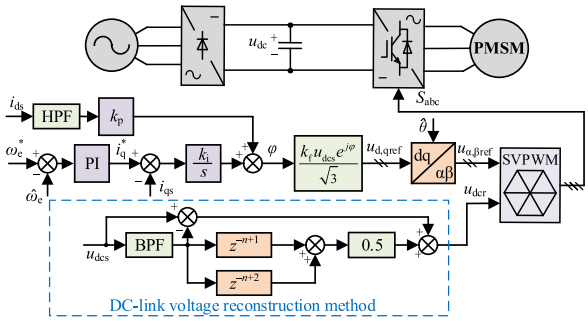

Fig. 3. Control block diagram of beat suppression method based on DC-link voltage reconstruction.

where $I_{d,q0}$ is the average of the dq-axis currents. $I_{\mathrm{d,qk}}$ and $\varphi_{\mathrm{d,qk}}$ are the amplitude and phase of the harmonic of the dq-axis currents at $6k\omega_{\mathrm{g}}$, respectively.

Assuming that the rotor position angle at the initial moment is 0, the motor a-phase current can be expressed as

$$\begin{aligned} i_{\mathrm{a}} &= i_{\mathrm{a0}} + \sum_{k=1}^{\infty} \left(i_{\mathrm{ak-}} + i_{\mathrm{ak+}}\right) \\ &= I_{\mathrm{a0}} \sin\left(\omega_{\mathrm{e}} t + \varphi_{\mathrm{a0}}\right) + \sum_{k=1}^{\infty} \left\{I_{\mathrm{ak-}} \sin\left[\left(6k\omega_{\mathrm{g}} - \omega_{\mathrm{e}}\right) t + \varphi_{\mathrm{ak-}}\right]\right. \\ &\quad \left. + I_{\mathrm{ak+}} \sin\left[\left(6k\omega_{\mathrm{g}} + \omega_{\mathrm{e}}\right) t + \varphi_{\mathrm{ak+}}\right]\right\} \end{aligned} \tag{5}$$

where i_{a0} and $i_{\mathrm{ak+,-}}$ are the fundamental component and the harmonics at $|6k\omega_{\mathrm{g}} \pm \omega_{\mathrm{e}}|$ of motor current, respectively. ω_{e} is the electrical angular velocity. I_{a0} and φ_{a0} are the amplitude and phase of i_{a0}, respectively. $I_{\mathrm{ak+,-}}$ and $\varphi_{\mathrm{ak+,-}}$ are the amplitude and phase of $i_{\mathrm{ak+,-}}$, respectively.

The schematic diagram of the motor current beat phenomenon caused by the harmonic of the dc-link voltage at $6\omega_{\mathrm{g}}$ is shown in Fig. 2. Among the harmonics of the dc-link voltage, the amplitude at $6\omega_{\mathrm{g}}$ is the largest, which mainly leads to the beat phenomenon. When the operating frequency is close to $6\omega_{\mathrm{g}}$, the lower frequency beat phenomenon caused by harmonic at $|6\omega_{\mathrm{g}} - \omega_{\mathrm{e}}|$ in the motor current is the main goal of beat suppression.

The amplitude of the beat envelope is proportional to the amplitude of the dc-link voltage harmonic [23]. Hence, under the same operating conditions, the smaller the capacitance of the dc-link, the more serious the beat phenomenon will be. In order to improve the performance and operational reliability of the drive system, it is necessary to suppress the beat phenomenon.

B. Analysis of Beat Phenomenon Under FW Control

When the motor is operating in FW region, it usually operates in the deep modulation region to ensure voltage utilization. At this time, due to the influence of the modulation range, the current loop cannot realize the effective control of the harmonics at the frequency of dc-link fluctuation, and the current harmonic problem is more serious. In the electrolytic capacitorless drives, the modulation index fluctuation problem will lead to a decrease in voltage utilization, especially in the deep modulation region [26], [27]. Hence, this article adopts the voltage angle FW control method proposed in [28] to reduce the influence of modulation index fluctuation.

The beat suppression method based on dc-link voltage reconstruction is commonly used, whose control block diagram is shown in Fig. 3 [20]. By predicting the average of dc-link voltage in the next switching cycle, the dc-link voltage sampling and calculation delay is eliminated, so that the actual output voltage is equal to the voltage reference, and the influence of dc-link voltage harmonics on the motor voltage is reduced, which suppresses the beat phenomenon in motor current. Using the periodicity of the dc-link voltage, the harmonics of the dc-link voltage sampling value at $6\omega_{\mathrm{g}}$ of one and two sampling periods ahead can be expressed as $u_{\mathrm{dcs6\omega g}} z^{-n+1}$ and $u_{\mathrm{dcs6\omega g}} z^{-n+2}$. Therefore, at the moments of $(\mathrm{n}+1)T_{\mathrm{s}}$ and $(\mathrm{n}+2)T_{\mathrm{s}}$, the predicted average of dc-link voltage u_{dcr} can be approximated as

$$u_{\mathrm{dcr}}(z) = U_{\mathrm{dc0}} + \frac{u_{\mathrm{dcs6\omega g}}(z) z^{-n+1} + u_{\mathrm{dcs6\omega g}}(z) z^{-n+2}}{2}. \tag{6}$$

When the motor operates in the FW region, the influence of dc-link voltage on motor current is complex, so it is necessary to establish the impedance model of the dc-link voltage and the motor currents under FW control, and quantitatively analyze the influence of the dc-link voltage harmonics on the beat phenomenon. As shown in Fig. 3, in the case of FW control, the dq-axis voltages are distributed by the voltage angle, and the dq-axis voltage references $u_{\mathrm{d,qref}}$ can be expressed as

$$\begin{cases} u_{\mathrm{dref}} = k_{\mathrm{f}} u_{\mathrm{dcs}} \cos\varphi / \sqrt{3} \\ u_{\mathrm{qref}} = k_{\mathrm{f}} u_{\mathrm{dcs}} \sin\varphi / \sqrt{3} \end{cases} \tag{7}$$

where φ is the voltage angle, k_{f} is the FW coefficient, and u_{dcs} is the sample value of dc-link voltage.

It can be seen from the dq-axis voltage reference equation that the amplitude of the motor voltage vector is proportional to the dc-link voltage, and the proportionality coefficient is the FW coefficient. From (7), the small signal variations of the dq-axis voltage references $\Delta u_{\mathrm{d,qref}}$ can be expressed as

$$\begin{aligned} \begin{bmatrix} \Delta u_{\mathrm{dref}} \\ \Delta u_{\mathrm{qref}} \end{bmatrix} &= \begin{bmatrix} -\sin\varphi_0 \\ \cos\varphi_0 \end{bmatrix} k_{\mathrm{f}} U_{\mathrm{dc0}} \Delta\varphi \Big/ \sqrt{3} \\ &\quad + \begin{bmatrix} \cos\varphi_0 \\ \sin\varphi_0 \end{bmatrix} k_{\mathrm{f}} T_{\mathrm{d}} \Delta u_{\mathrm{dc}} \Big/ \sqrt{3} \end{aligned} \tag{8}$$

where φ_0 is the average of the voltage angle, and T_d is the delay function with a delay of 0.5 sampling periods. $\Delta\varphi$ and Δu_dc are the small signal variations of the voltage angle and dc-link voltage, respectively.

However, due to the delay in sampling and calculating of the dc-link voltage, there is a deviation between the actual *dq*-axis voltages and its references. The relationship between the actual *dq*-axis voltages $\Delta u_{\mathrm{d,q}}$ and its references can be expressed as

$$\begin{bmatrix}\Delta u_\mathrm{d}\\ \Delta u_\mathrm{q}\end{bmatrix}=\begin{bmatrix}\Delta u_\mathrm{dref}\\ \Delta u_\mathrm{qref}\end{bmatrix}+\frac{\left(1-e^{-1.5sT_\mathrm{s}}\right)\Delta u_\mathrm{dc}}{U_\mathrm{dc0}}\begin{bmatrix}U_\mathrm{d0}\\ U_\mathrm{q0}\end{bmatrix} \tag{9}$$

where $U_{\mathrm{d,q0}}$ and T_s are the average of the *dq*-axis voltages and the switching cycle, respectively.

In order to analyze the beat phenomenon of the system, it is necessary to establish the admittance relationship between the motor current and the dc-link voltage. According to the control block diagram, $\Delta\varphi$ can be expressed as

$$\Delta\varphi=\begin{bmatrix}K_\mathrm{p}\boldsymbol{G}_\mathrm{HPF} & -\frac{K_\mathrm{i}}{s}\end{bmatrix}\begin{bmatrix}\Delta i_\mathrm{d}\\ \Delta i_\mathrm{q}\end{bmatrix}T_\mathrm{d} \tag{10}$$

where $\Delta i_{\mathrm{d,q}}$ are the small signal variations of the *dq*-axis currents, K_i is the coefficient of the *q*-axis current regulator, K_p is the gain of the *d*-axis current compensation, and $\boldsymbol{G}_\mathrm{HPF}$ is the transfer function of the high-pass filter.

Combined with (8), (9), (10) and the voltage equation, the transfer function $\boldsymbol{W}_{\mathrm{d,q}\varphi}$ between the *dq*-axis currents and the dc-link voltage under FW control can be expressed as

$$\begin{bmatrix}\boldsymbol{W}_{\mathrm{d}\varphi}\\ \boldsymbol{W}_{\mathrm{q}\varphi}\end{bmatrix}=\frac{1}{\Delta u_\mathrm{dc}}\begin{bmatrix}\Delta i_\mathrm{d}\\ \Delta i_\mathrm{q}\end{bmatrix}=\boldsymbol{X}^{-1}\boldsymbol{Y}=\boldsymbol{X}^{-1}\left(\boldsymbol{Y}_\mathrm{VST}+\boldsymbol{Y}_\mathrm{FWC}\right) \tag{11}$$

where the matrices $\boldsymbol{X}$, $\boldsymbol{Y}_\mathrm{VST}$, and $\boldsymbol{Y}_\mathrm{FWC}$ are

$$\begin{cases}\boldsymbol{X}_{11}=R_\mathrm{s}+L_\mathrm{d}s+K_\mathrm{p}\boldsymbol{G}_\mathrm{HPF}U_\mathrm{dc0}\sin\varphi_0T_\mathrm{d}k_\mathrm{f}/\sqrt{3}\\ \boldsymbol{X}_{12}=-\omega_\mathrm{e}L_\mathrm{q}-K_\mathrm{i}U_\mathrm{dc0}\sin\varphi_0T_\mathrm{d}k_\mathrm{f}/\left(\sqrt{3}s\right)\\ \boldsymbol{X}_{21}=\omega_\mathrm{e}L_\mathrm{d}-K_\mathrm{p}\boldsymbol{G}_\mathrm{HPF}U_\mathrm{dc0}\cos\varphi_0T_\mathrm{d}k_\mathrm{f}/\sqrt{3}\\ \boldsymbol{X}_{22}=R_\mathrm{s}+L_\mathrm{q}s+K_\mathrm{i}U_\mathrm{dc0}\cos\varphi_0T_\mathrm{d}k_\mathrm{f}/\left(\sqrt{3}s\right)\end{cases} \tag{12}$$

$$\boldsymbol{Y}_\mathrm{VST}=\begin{bmatrix}\frac{\left(1-e^{-1.5sT_\mathrm{s}}\right)U_\mathrm{d0}}{U_\mathrm{dc\_0}}\\ \frac{\left(1-e^{-1.5sT_\mathrm{s}}\right)U_\mathrm{q0}}{U_\mathrm{dc0}}\end{bmatrix},\boldsymbol{Y}_\mathrm{FWC}=\begin{bmatrix}\frac{\cos\varphi_0T_\mathrm{d}k_\mathrm{f}}{\sqrt{3}}\\ \frac{\sin\varphi_0T_\mathrm{d}k_\mathrm{f}}{\sqrt{3}}\end{bmatrix} \tag{13}$$

where R_s and $L_{\mathrm{d,q}}$ are the stator resistance and the *dq*-axis inductances, respectively.

From (11) and (13), the admittance between the motor currents and the dc-link voltage is affected by two parts. The one part is VST-A that exists in the entire operating range, corresponding to $\boldsymbol{X}^{-1}\boldsymbol{Y}_\mathrm{VST}$, which is caused by the sampling and calculation delay in the dc-link voltage. The other part is FWC-A, corresponding to $\boldsymbol{X}^{-1}\boldsymbol{Y}_\mathrm{FWC}$. After the dc-link voltage reconstruction method completely eliminates the sampling and calculation errors, the exponent of e in $\boldsymbol{Y}_\mathrm{VST}$ will be 0, and then VST-A is eliminated. As shown in Fig. 4, the voltage reconstruction method can suppress the admittance between the motor currents and the dc-link voltage to a certain extent during the FW operation. When the motor operates at the frequency of 390 Hz and the load torque is 21 N·m, the *dq*-axis admittances decrease by 1.51 dB and 1.50 dB, respectively. However, due to FWC-A, the admittance suppression effect of this method is limited.

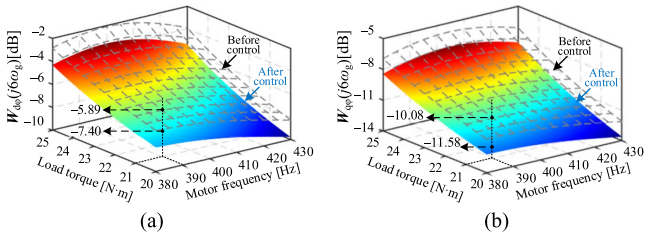

Fig. 4. Amplitude of the transfer function at $6\omega_\mathrm{g}$ before and after applying the voltage reconstruction method. (a) $W_{\mathrm{d}\varphi}(j6\omega_\mathrm{g})$. (b) $W_{\mathrm{q}\varphi}(j6\omega_\mathrm{g})$.

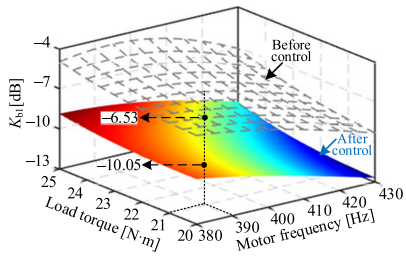

Fig. 5. Ratio of the beat amplitude to the fundamental amplitude.

According to (11) and the analysis in [23], the ratio K_bk of the amplitude of beat current caused by the dc-link voltage harmonic at $6k\omega_\mathrm{g}$ to the fundamental amplitude of the motor current can be expressed as

$$K_\mathrm{bk}=\frac{\left|I_\mathrm{d0}\mathbf{W}_{\mathrm{d}\varphi}\left(j6k\omega_\mathrm{g}\right)+I_\mathrm{q0}\mathbf{W}_{\mathrm{q}\varphi}\left(j6k\omega_\mathrm{g}\right)\right|}{I_\mathrm{a0}^2}U_\mathrm{dck}. \tag{14}$$

Combined with (11) and (14), the ratio K_b1 of the amplitude of beat current caused by the dc-link voltage harmonic at $6\omega_\mathrm{g}$ to the fundamental amplitude of the motor current is shown in Fig. 5. When the motor frequency is 390 Hz and the load torque is 21 N·m, K_b1 is –6.53 dB, and the ratio is reduced to –10.05 dB after the dc-link voltage reconstruction method is adopted, which is limited. In order to improve the beat suppression effect of electrolytic capacitorless drives, it is necessary to further reduce FWC-A.

III. Proposed Beat Suppression Strategy Based on Voltage Angle Harmonic Regulation

A. Principle of Voltage Angle Harmonic Regulation

In order to reduce FWC-A of the electrolytic capacitorless drives, a beat suppression strategy based on the adaptive regulation of voltage angle harmonic is proposed, and the control block diagram is shown in Fig. 6. According to the motor speed and the average value of the *dq*-axis currents, the adaptive control is to obtain the real and imaginary parts of the numerator denominator of the transfer function $\boldsymbol{G}_\mathrm{mad}(s)$ at $6\omega_\mathrm{g}$ through the impedance relation (20). The relationship of amplitude and phase between voltage angle and dc-link voltage at the minimum amplitude of the beat current can be obtained. Then, the parameters of the harmonic regulation of the voltage angle can be obtained through (25). The harmonic regulation is based on the dc-link voltage

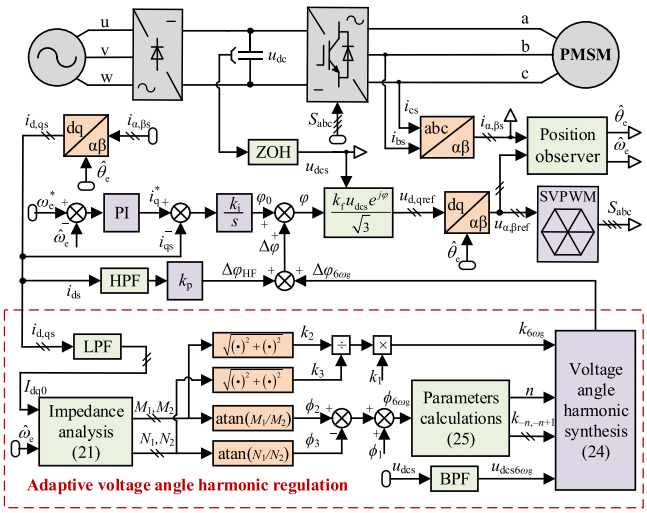

Fig. 6. Block diagram of the beat suppression strategy of adaptive voltage angle harmonic regulation.

at $6\omega_g$, and the expected voltage angle harmonic is obtained by delay processing and amplitude adjustment. The generated angle harmonic is superimposed on the voltage angle to changes the admittance relationship between the motor currents and the dc-link voltage, which reduces FWC-A and further suppresses the beat phenomenon.

By analyzing the admittance relationship between the motor currents and the dc-link voltage after control, the control mechanism of voltage phase angle harmonic regulation can be clarified. The beat phenomenon of motor current is mainly caused by the dc-link voltage harmonic at $6\omega_g$, in order to simplify the analysis, only the response of the system to $6\omega_g$ is considered. Combining (8) and the motor voltage equation, the transfer function between the *dq*-axis currents and the dc-link voltage at $6\omega_g$ can be obtained

$$\begin{bmatrix} \boldsymbol{W}_{d\varphi} \\ \boldsymbol{W}_{q\varphi} \end{bmatrix} = \frac{1}{\Delta u_{dc}} \begin{bmatrix} \Delta i_d \\ \Delta i_q \end{bmatrix} = \boldsymbol{A}^{-1}\boldsymbol{B} \tag{15}$$

where the matrices $\boldsymbol{A}$ and $\boldsymbol{B}$ are

$$\begin{cases} \boldsymbol{A}_{11} = R_s + L_d s \\ \boldsymbol{A}_{12} = -\omega_e L_q \\ \boldsymbol{A}_{21} = \omega_e L_d \\ \boldsymbol{A}_{22} = R_s + L_q s \end{cases} \tag{16}$$

$$\begin{cases} \boldsymbol{B}_{11} = k_f \frac{-\sin(\varphi_0) U_{dc0} \boldsymbol{G}_{mad} + T_d \cos\varphi_0}{\sqrt{3}} + \frac{\left(1-e^{-1.5sT_s}\right)U_{d0}}{U_{dc0}} \\ \boldsymbol{B}_{21} = k_f \frac{\cos(\varphi_0) U_{dc0} \boldsymbol{G}_{mad} + T_d \sin\varphi_0}{\sqrt{3}} + \frac{\left(1-e^{-1.5sT_s}\right)U_{q0}}{U_{dc0}} \end{cases} \tag{17}$$

where $\boldsymbol{G}_{mad}(s)$ is the transfer function between the voltage angle and the dc-link voltage at $6\omega_g$.

Compared with (13) and (17), the proposed method will change the original admittance relationship between the motor current and the dc-link voltage at $6\omega_g$, and FWC-A and the amplitude of motor current beat envelope can be reduced by designing $\boldsymbol{G}_{mad}(s)$. Combined with (14), when the beat phenomenon caused by the harmonic of dc-link voltage at $6\omega_g$ is completely suppressed, the following relationship is obtained:

$$I_{d0}\left(\boldsymbol{A}_{22}\boldsymbol{B}_{11} - \boldsymbol{A}_{12}\boldsymbol{B}_{21}\right) + I_{q0}\left(-\boldsymbol{A}_{21}\boldsymbol{B}_{11} + \boldsymbol{A}_{11}\boldsymbol{B}_{21}\right) = 0. \tag{18}$$

According to (18), the transfer function $\boldsymbol{G}_{mad}(s)$ between the voltage angle and the dc-link voltage can be expressed as

$$\begin{aligned} &\boldsymbol{G}_{mad} \\ &= \frac{U_{d0}\left(e^{-0.5sT_s} + 1 - e^{-1.5sT_s}\right)\left(I_{q0}\boldsymbol{A}_{21} - I_{d0}\boldsymbol{A}_{22}\right)}{U_{dc0}\left[\left(I_{q0}\boldsymbol{A}_{11} - I_{d0}\boldsymbol{A}_{12}\right)U_{d0} - \left(I_{d0}\boldsymbol{A}_{22} - I_{q0}\boldsymbol{A}_{21}\right)U_{q0}\right]} \\ &\quad + \frac{U_{q0}\left(e^{-0.5sT_s} + 1 - e^{-1.5sT_s}\right)\left(I_{d0}\boldsymbol{A}_{12} - I_{q0}\boldsymbol{A}_{11}\right)}{U_{dc0}\left[\left(I_{q0}\boldsymbol{A}_{11} - I_{d0}\boldsymbol{A}_{12}\right)U_{d0} - \left(I_{d0}\boldsymbol{A}_{22} - I_{q0}\boldsymbol{A}_{21}\right)U_{q0}\right]}. \end{aligned} \tag{19}$$

According to the abovementioned analysis, the transfer function $\boldsymbol{G}_{mad}(s)$ with the lowest amplitude of beat envelope contains the motor operation information and parameter information. In order to simplify the analysis and ignore the stator resistance voltage drop, according to the voltage equation and (19), the response of the transfer function $\boldsymbol{G}_{mad}(s)$ at $6\omega_g$ can be expressed as

$$\boldsymbol{G}_{mad}\left(j6\omega_g\right) = \frac{\left(e^{-j9\omega_g T_s} - e^{-j3\omega_g T_s} - 1\right)\left(j\boldsymbol{M}_1 + \boldsymbol{M}_2\right)}{U_{dc0}\left(j\boldsymbol{N}_1 + \boldsymbol{N}_2\right)} \tag{20}$$

where $\boldsymbol{M}_{1,2}$ and $\boldsymbol{N}_{1,2}$ in the numerator and denominator are

$$\begin{cases} \boldsymbol{M}_1 = \left[\left(L_d^2 - L_q^2\right) I_{d0} I_{q0} + L_d I_{q0} \psi_f\right] 6\omega_g \\ \boldsymbol{M}_2 = \omega_e L_d L_q \left(I_{d0}^2 + I_{q0}^2\right) + \omega_e \psi_f L_q I_{d0} \\ \boldsymbol{N}_1 = \left[-\left(L_d L_q \left(I_{d0}^2 + I_{q0}^2\right) + L_q I_{d0} \psi_f\right)\right] 6\omega_g \\ \boldsymbol{N}_2 = \omega_e \left(L_d^2 - L_q^2\right) I_{d0} I_{q0} + \omega_e \psi_f L_d I_{q0} \end{cases} \tag{21}$$

where ψ_f is flux of permanent magnets.

From the abovementioned analysis, (21) contains information about the motor currents and motor speed, so the control method can adaptively regulate the harmonic of the voltage angle according to the operating conditions. According to Euler's formula, when the amplitude of beat envelope is minimum, the relationship of amplitude and phase between the voltage angle and the dc-link voltage at $6\omega_g$ can be expressed as

$$\begin{cases} k_{6\omega_g} = \left|\boldsymbol{G}_{mad}\left(j6\omega_g\right)\right| = k_1 k_2 / k_3 \\ \phi_{6\omega_g} = \angle \boldsymbol{G}_{mad}\left(j6\omega_g\right) = \phi_1 + \phi_2 - \phi_3 \end{cases} \tag{22}$$

where $k_{6\omega g}$ and $\phi_{6\omega g}$ are the amplitude ratio and phase difference of the voltage angle and the dc-link voltage at $6\omega_g$, respectively. $k_{1,2,3}$ and $\phi_{1,23}$ can be expressed as

$$\begin{cases} k_1 = \left|\frac{e^{-j9\omega_g T_s} - e^{-j3\omega_g T_s} - 1}{U_{dc0}}\right|, \phi_1 = \angle\left(\frac{e^{-j9\omega_g T_s} - e^{-j3\omega_g T_s} - 1}{U_{dc0}}\right) \\ k_2 = \sqrt{\boldsymbol{M}_1{}^2 + \boldsymbol{M}_2{}^2}, \phi_2 = \arctan\left(\boldsymbol{M}_1 / \boldsymbol{M}_2\right) \\ k_3 = \sqrt{\boldsymbol{N}_1{}^2 + \boldsymbol{N}_2{}^2}, \phi_3 = \arctan\left(\boldsymbol{N}_1 / \boldsymbol{N}_2\right). \end{cases} \tag{23}$$

According to the amplitude and phase relationship between the voltage angle and the dc-link voltage at $6\omega_g$, the harmonic $\varphi_{6\omega g}$ of the voltage angle at $6\omega_g$ can be synthesized by the delayed harmonic of the dc-link voltage, as shown in Fig. 7.

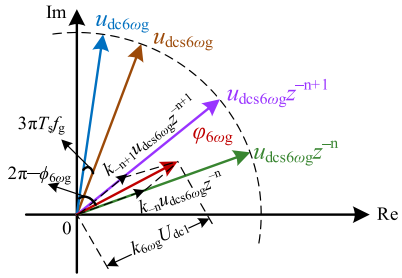

Fig. 7. Vector diagram of voltage angle harmonic synthesis.

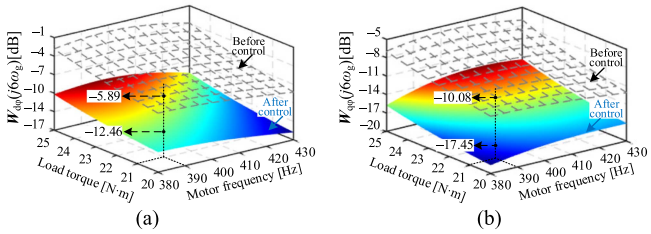

Fig. 8. Amplitude of the transfer function at $6\omega_g$ before and after applying the proposed method. (a) $W_{d\varphi}(j6\omega_g)$. (b) $W_{q\varphi}(j6\omega_g)$.

Then, the discrete expression of the voltage angle harmonic regulation can be obtained

$$\varphi_{6\omega g}(z) = k_{6\omega g}\left(k_{-n}u_{dcs6\omega g}(z)z^{-n} + k_{-n+1}u_{dcs6\omega g}(z)z^{-n+1}\right) \tag{24}$$

where n is the delay period, and $k_{-n,\,-n+1}$ is the corresponding gain.

According to (23) and Fig. 7, the parameters in (24) are

$$\begin{cases} n = \left\lceil \dfrac{2\pi-\phi_{6\omega_g}}{12\pi T_s f_g} - 0.5 \right\rceil \\ k_{-n} = \dfrac{\sin\left[(n-0.5)12\pi T_s f_g + \phi_{6\omega_g}\right]}{\sin(-12\pi T_s f_g)} \\ k_{-n+1} = \dfrac{\sin\left[(n+0.5)12\pi T_s f_g + \phi_{6\omega_g}\right]}{\sin(12\pi T_s f_g)} \end{cases} \tag{25}$$

where the symbol $\lceil\rceil$ is the rounding up, and f_g is the grid frequency.

B. Analysis of the Adaptability and Stability

The admittance relationship between the *dq*-axis currents and the dc-link voltage at $6\omega_g$ after the application of the proposed method is shown in Fig. 8. The *dq*-axis admittance is further suppressed by the proposed method compared to Fig. 4. When the motor frequency is 390 Hz and the load torque is 21 N·m, the dq admittances decrease by 6.57 dB and 7.37 dB, respectively. That is, the proposed method can suppress the FWC-A and reduce the current harmonics.

In order to analyze the suppression effect on the motor current beat phenomenon in FW region, the proposed method is compared with the beat suppression method proposed in [20]. After the application of the proposed method, the ratio of the amplitude of the motor current beat envelope to the fundamental amplitude of the motor current under different working conditions is shown in Fig. 9. When the motor frequency is 390 Hz

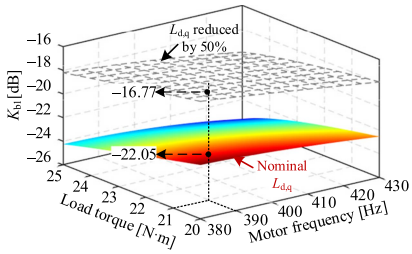

Fig. 9. Beat suppression effect of the proposed method under parameters change.

and the load torque is 21 N·m, K_{b1} is –22.05 dB. Compared with the voltage reconstruction algorithm in Fig. 5, the amplitude of beat envelope is reduced by 12 dB. Due to the simplification of the resistor voltage drop in the analysis, the proposed method cannot suppress the beat current to 0 A. However, the proposed method has a better suppression effect than the beat suppression method proposed in [20], and it is still effective when the motor parameters change. The proposed method regulates the voltage angle harmonic according to the dc-link voltage, so the proposed method is not sensitive to the inverter parameters and has satisfactory robustness.

From Fig. 1, the electrolytic capacitorless system can be regarded as a cascade system composed of an RLC filter and an inverter, and the stability of the system after applying the proposed method can be analyzed according to the Nyquist criterion of the impedance of PMSM and the filter. The above analysis is only for the response of the system to $6\omega_g$, so the matrix $\boldsymbol{Y}$ is substituted with matrix $\boldsymbol{Z}$ in (11) when the proposed method is adopted

$$\begin{bmatrix} \boldsymbol{W}_{d\varphi} \\ \boldsymbol{W}_{q\varphi} \end{bmatrix} = \frac{1}{\Delta u_{dc}} \begin{bmatrix} \Delta i_d \\ \Delta i_q \end{bmatrix} = \boldsymbol{X}^{-1}\boldsymbol{Z} \tag{26}$$

where the elements in the matrix Z are

$$\begin{cases} \boldsymbol{Z}_{11} = k_f \dfrac{-U_{q0}\boldsymbol{G}_{mad}\boldsymbol{G}_{BPF} + T_d\cos\varphi_0}{\sqrt{3}} + \dfrac{\left(1-e^{-1.5sT_s}\right)U_{d0}}{U_{dc0}} \\ \boldsymbol{Z}_{21} = k_f \dfrac{U_{d0}\boldsymbol{G}_{mad}\boldsymbol{G}_{BPF} + T_d\sin\varphi_0}{\sqrt{3}} + \dfrac{\left(1-e^{-1.5sT_s}\right)U_{q0}}{U_{dc0}} \end{cases} \tag{27}$$

where $\boldsymbol{G}_{BPF}$ is the transfer function of the bandpass filter. According to the experimental system parameters, the center frequency of the bandpass filter is set to $6\omega_g$. The transfer functions $\boldsymbol{G}_{BPF}(s)$ of the bandpass filter can be expressed as

$$\boldsymbol{G}_{BPF}(s) = \frac{6\xi_1\omega_g s}{s^2 + 6\xi_1\omega_g s + 36\omega_g^2} \tag{28}$$

where ξ_1 is the bandwidth of the bandpass filter. The utility grid is not entirely ideal, and the frequency of the grid fluctuates within a certain range. In order to ensure that the filter can effectively filter out the harmonic of the dc-link voltage at $6\omega_g$, it is necessary to set sufficient bandwidth of 20 Hz.

The input admittance of inverter can be expressed as

$$\boldsymbol{Y}_m = \frac{\Delta i_{inv}}{\Delta u_{dc}} = \frac{3\boldsymbol{W}_{d\varphi}\left(U_{d0} + \omega_e L_d I_{q0} + L_d I_{d0} s + I_{d0}R_s\right)}{2U_{dc0}}$$

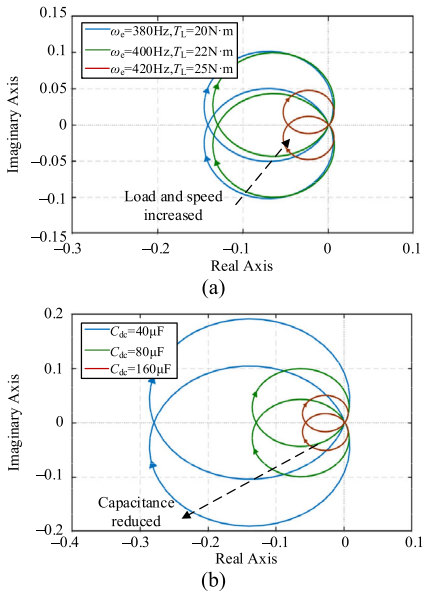

Fig. 10. Nyquist diagram of $Y_{\mathrm{m}}/Y_{\mathrm{RLC}}$. (a) Changes in operating conditions. (b) Changes in DC-link capacitance.

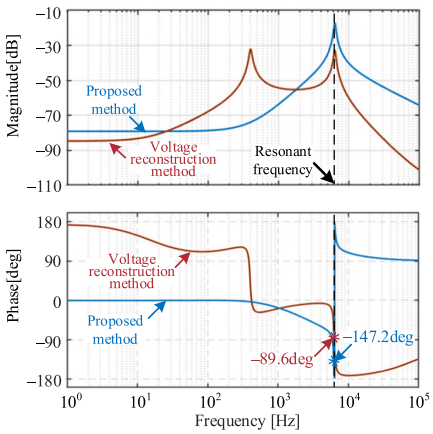

Fig. 11. Bode diagram of $Y_{\mathrm{m}}/Y_{\mathrm{RLC}}$.

$$+\frac{3\boldsymbol{W}_{\mathrm{q}\varphi}\left(U_{\mathrm{q0}}-\omega_{\mathrm{e}}L_{\mathrm{q}}I_{\mathrm{d0}}+L_{\mathrm{q}}I_{\mathrm{q0}}s+I_{\mathrm{q0}}R_{\mathrm{s}}\right)}{2U_{\mathrm{dc0}}}-\frac{I_{\mathrm{inv0}}}{U_{\mathrm{dc0}}} \tag{29}$$

where i_{inv} and I_{inv0} are the input current of the inverter and its average, respectively.

The dc side admittance $\boldsymbol{Y}_{\mathrm{RLC}}$ can be expressed as

$$\boldsymbol{Y}_{\mathrm{RLC}}=\left(L_{\mathrm{eq}}C_{\mathrm{dc}}s^2+R_{\mathrm{g}}C_{\mathrm{dc}}s+1\right)/\left(L_{\mathrm{eq}}s+R_{\mathrm{g}}\right). \tag{30}$$

From the abovementioned analysis, the stability of the system can be judged by the Nyquist diagram of $\boldsymbol{Y}_{\mathrm{m}}/\boldsymbol{Y}_{\mathrm{RLC}}$, as shown in Fig. 10. As the motor speed and load increase, the Nyquist curve of $\boldsymbol{Y}_{\mathrm{m}}/\boldsymbol{Y}_{\mathrm{RLC}}$ does not contain $(-1,0)$, so the system is stable. As the dc-link capacitance decreases, the Nyquist curve of $\boldsymbol{Y}_{\mathrm{m}}/\boldsymbol{Y}_{\mathrm{RLC}}$ does not contain $(-1,0)$.

The Bode diagram of $\boldsymbol{Y}_{\mathrm{m}}/\boldsymbol{Y}_{\mathrm{RLC}}$ is shown in Fig. 11. The amplitude of $\boldsymbol{Y}_{\mathrm{m}}/\boldsymbol{Y}_{\mathrm{RLC}}$ is maximum around the resonant frequency. The phase margins of the dc-link voltage reconstruction method is 90.4° at the frequency with the largest amplitude, and the phase margins of the proposed method is 32.8°. When the proposed method is applied, the stability of the system can be guaranteed.

TABLE I
CHARACTERISTICS OF THE BEAT SUPPRESSION METHODS

Criteria	*Voltage reconstruction method*	*Proposed method*
Beat suppression	★★	★★★
Stability	★★★	★★★
Parameter sensitivity	★★★	★★

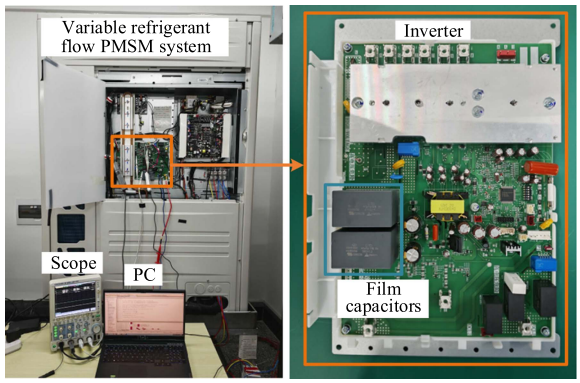

Fig. 12. Experimental platform of electrolytic capacitorless variable refrigerant flow PMSM system.

The characteristics of the beat suppression methods are shown in Table I. Compared with the dc-link voltage reconstruction method, the proposed method has a better beat suppression effect. Although the sensitivity to the parameters of the proposed method is slightly inferior to the dc-link voltage reconstruction method, the system has satisfactory robustness to the parameters.

IV. EXPERIMENTAL RESULTS

The experimental platform takes the permanent magnet compressor as the control object. The dc-link capacitance is 80 μF, the ac input of the inverter is 380-Vrms (50 Hz), the inverter power is 13.5 kW, and the motor parameters L_{d}, L_{q} R_{s}, pole pair, flux of permanent magnet, and inertia are 2.5 mH, 2.9 mH, 0.115 Ω, 3, 0.1575 Wb, and 0.00322 kg·m^2 respectively. The inverter is controlled by a Renesas chip RX66T, and the switching and sampling frequency is set to 5 kHz. The experimental platform is shown in Fig. 12.

The experimental results at compressor frequency of 390 Hz are shown in Fig. 13. As shown in Fig. 13(a), the amplitude of the motor current decreases after the voltage reconstruction method is applied. After the application of the proposed method, additional fluctuations are introduced in the voltage angle and the amplitude of motor current decreases further. As can be seen from Fig. 13(b) and (c), compared with the voltage reconstruction method, the proposed method introduces additional harmonics into the voltage angle, which changes the

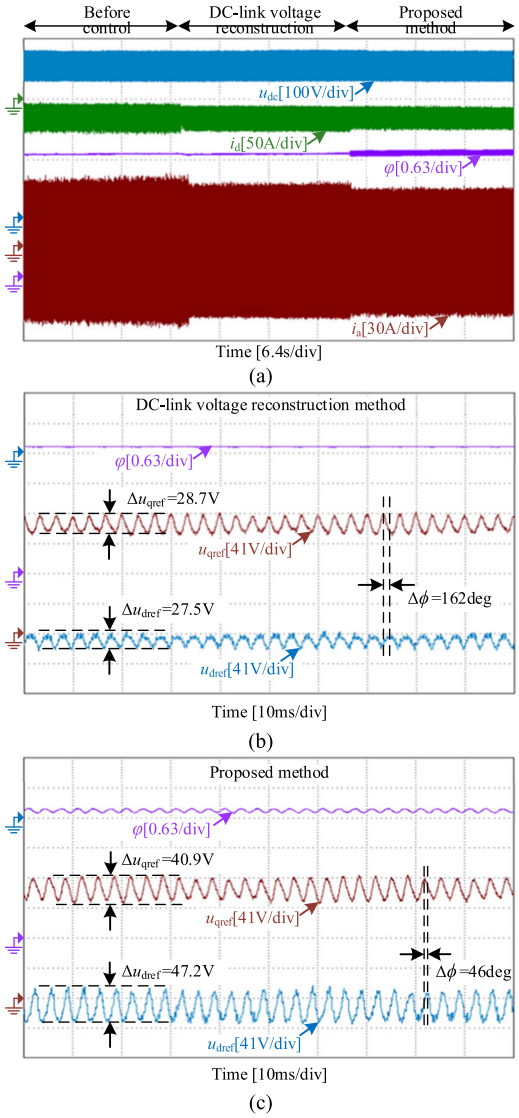

Fig. 13. Experimental results at compressor frequency of 390 Hz. (a) Experimental results under different methods. (b) With the voltage reconstruction method. (c) With the proposed method.

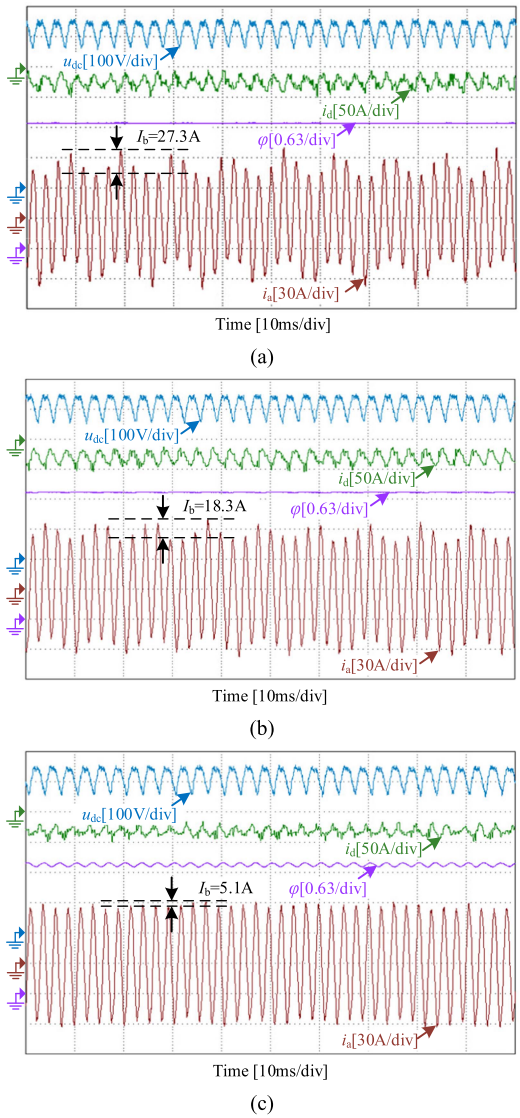

Fig. 14. Enlarged experimental results at compressor frequency of 390 Hz. (a) Without beat phenomenon suppression method. (b) With the voltage reconstruction method. (c) With the proposed method.

impedance characteristics. The fluctuations of the *dq*-axis voltages are increased from 27.5 V and 28.7 V to 47.2 V and 40.9 V, respectively. The phase difference between the *dq*-axis voltages is decreased from 162° to 46°. By regulating the harmonic of voltage angle, the harmonics of *dq*-axis voltages are adjusted, and then the harmonic of motor current is suppressed.

The enlarged experimental results at compressor frequency of 390 Hz are shown in Fig. 14. The waveforms from top to bottom are the dc-link voltage, the d-axis current, voltage angle, and a-phase current, respectively. As can be seen from Fig. 14(a), (b), and (c), the amplitude of the motor current beat envelope is 27.3 A without beat phenomenon suppression strategy, and it is reduced to 18.3 A after the dc-link voltage reconstruction method is applied. After the proposed method is applied, the amplitude of the motor current beat envelope is further reduced to 5.1 A.

Fig. 15 shows the FFT results of the motor current at compressor frequency of 390 Hz. As can be seen from Fig. 15(a), (b), and (c), the amplitude of the motor current harmonic I_{a1-} at the frequency of $|6\omega_g - \omega_e|$ without beat phenomenon suppression strategy is 7.0 A. I_{a1-} is reduced to 5.2 A and 2.4 A after the dc-link voltage reconstruction method and the proposed method is applied, respectively. In addition, the THD of the motor current is reduced from 25.0% to 22.3% and 13.3% after the dc-link voltage reconstruction method and the proposed method is applied, respectively.

Fig. 16 shows the compressor frequency and electromagnetic torque waveforms at compressor frequency of 390 Hz. Compared to the dc-link voltage reconstruction method, the proposed method results in lower fluctuations in motor speed and electromagnetic torque. The speed fluctuation is decreased from 18.1 Hz to 16.8 Hz, and the electromagnetic torque fluctuation decreases from 7.5 N·m to 3.9 N·m.

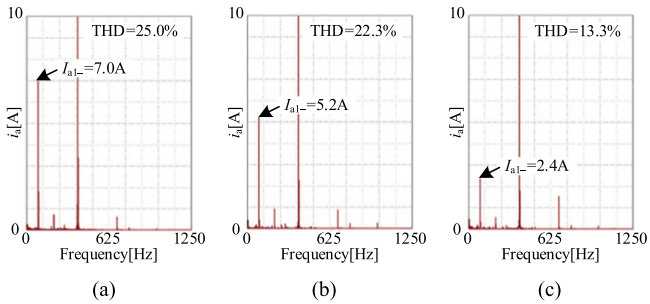

Fig. 15. FFT results of the motor current at compressor frequency of 390 Hz. (a) Without beat phenomenon suppression method. (b) With the voltage reconstruction method. (c) With the proposed method.

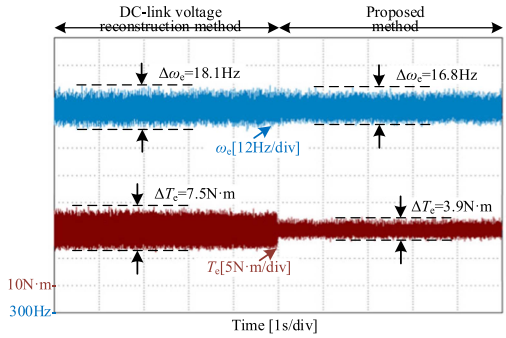

Fig. 16. Compressor frequency and electromagnetic torque waveforms at compressor frequency of 390 Hz.

The experimental results of compressor frequency from 380 Hz to 420 Hz are shown in Fig. 17. The waveforms from top to bottom are the dc-link voltage, the electromagnetic torque, voltage angle, and a-phase current, respectively. Fig. 17(a) and (b) are the experimental results of the dc-link voltage reconstruction method, and Fig. 17(b) shows that when the compressor frequency is 420 Hz, the amplitude of the motor current beat envelope is 15.8 A, and the electromagnetic torque fluctuation is 8.2 N·m. Fig. 17(c) and (d) is the experimental results of the proposed method, and Fig. 17(d) shows that when the compressor frequency is 420 Hz, the amplitude of the motor current beat envelope is 7.9 A, and the electromagnetic torque fluctuation is 6.5 N·m. Compared with the beat suppression method of dc-link voltage reconstruction, the acceleration and steady state of the motor under the proposed method have lower amplitude of motor current, amplitude of beat envelope and electromagnetic torque fluctuation.

Fig. 18 shows the FFT results of the motor current at compressor frequency of 420 Hz. As can be seen from Fig. 18(a) and (b), the amplitude of the motor current harmonic at $|6\omega_g - \omega_e|$ I_{a1-} is 3.6 A and 1.4 A after the dc-link voltage reconstruction method and the proposed method is applied, respectively. And the THD of the motor current is 22.5% and 19.0% after the dc-link voltage reconstruction method and the proposed method is applied, respectively. The proposed method has a better harmonic suppression effect.

The proposed beat suppression method is applied to permanent magnet compressors in HVAC applications, which usually does not have quick dynamic operating condition. The response

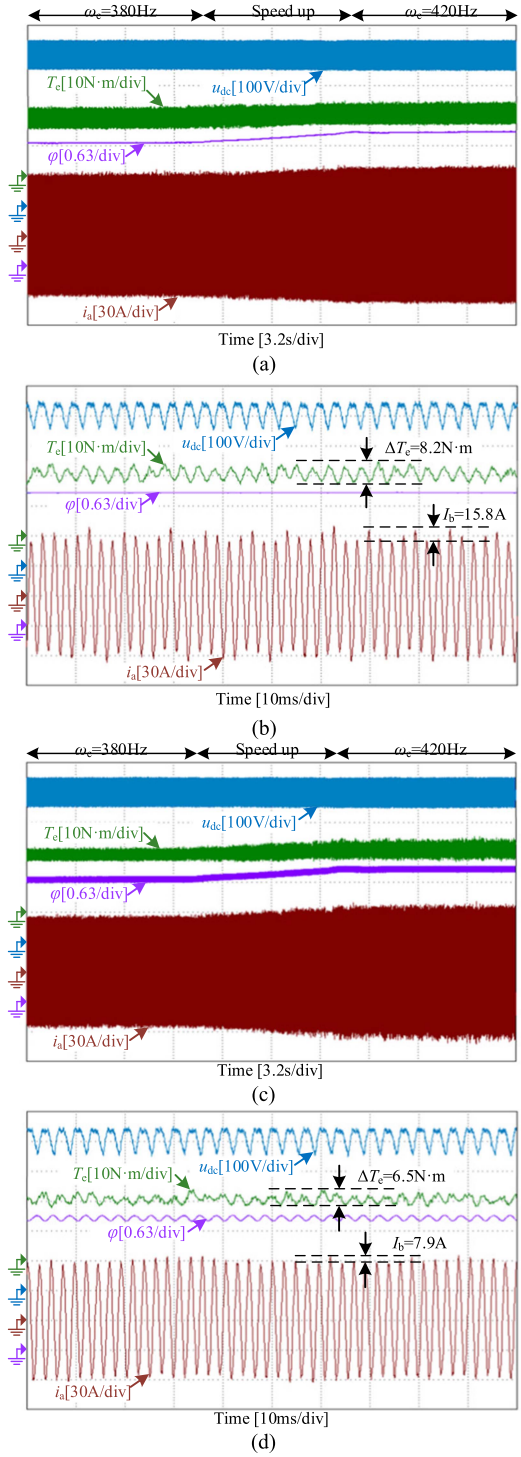

Fig. 17. Experimental results of compressor frequency from 380 Hz to 420 Hz. (a) With the voltage reconstruction method. (b) Enlarged view of the voltage reconstruction method at 420 Hz. (c) With the proposed method. (d) Enlarged view of the proposed method at 420 Hz.

speed can be analyzed by the time from enabling the algorithm to the steady state. As shown in Fig. 19, after the dc-link voltage reconstruction method is enabled, the system reaches the steady state time of 16 ms, and the proposed method is 17 ms. After applying the proposed method, the execution time of the algorithm in an interrupt is 24.58 μs, which is slightly higher

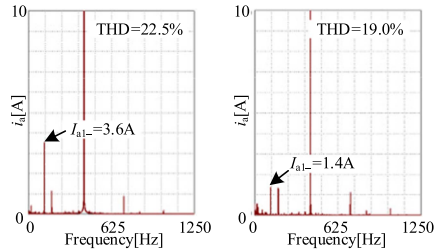

Fig. 18. FFT results of the motor current at compressor frequency of 420 Hz. (a) With the voltage reconstruction method. (b) With the proposed method.

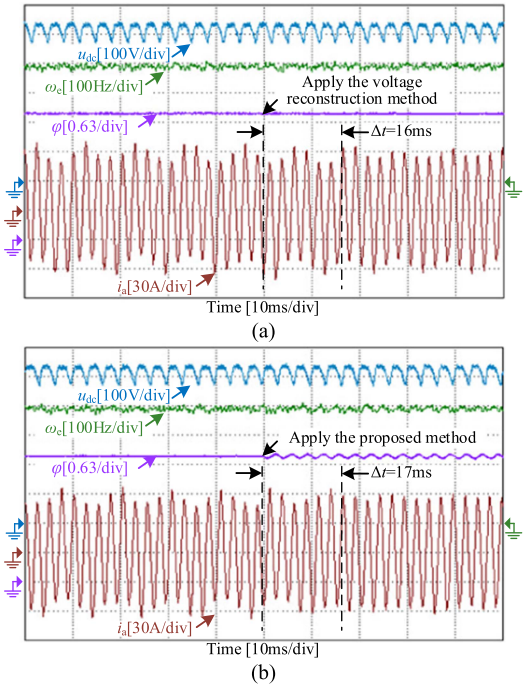

Fig. 19. Experimental results enabled by the beat suppression methods. (a) With the voltage reconstruction method. (b) With the proposed method.

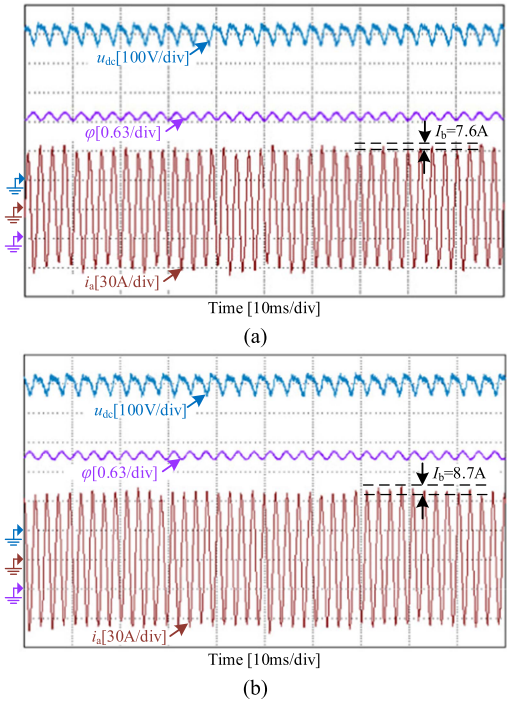

Fig. 20. Experimental results of changing the motor parameters in controller to twice. (a) Compressor frequency of 390 Hz. (b) Compressor frequency of 420 Hz.

TABLE II
CHARACTERISTICS OF THE BEAT SUPPRESSION METHODS

Criteria	*Original*	*Voltage reconstruction method*	*Proposed method*
Amplitude of motor current beat envelope [A]	23.4	15.2	6.4
THD of motor current [%]	23.9	21.7	16.2
Amplitude of motor current harmonic at $\lvert 6\omega_g - \omega_e \rvert$ [A]	5.5	3.9	1.7

than the dc-link voltage reconstruction method with 22.63 μs. The proposed method has sufficient response speed to ensure real-time control performance.

The motor parameters $L_{d,q}$ in the impedance analysis of the proposed method, which is shown in Fig. 6, are doubled to compare and analyze the sensitivity and the experimental results are shown in Fig. 20. Compared with Fig. 14(c) and Fig. 17(d), when the motor parameters in the Impedance analysis are doubled, the beat suppression ability decreases, and the amplitude of beat envelope is increased from 5.1 A to 7.6 A at compressor frequency of 390 Hz, and from 7.9 A to 8.7 A at compressor frequency of 420 Hz. The proposed method still has a satisfactory beat suppression effect under the inaccurate motor parameters.

The experimental statistical results of harmonic suppression ability of motor current in FW region are shown in Table II. The amplitude of beat envelope is decreased by an average of 34.9%, and 72.8% with the dc-link voltage reconstruction method and the proposed method, respectively. THD of motor current is decreased by an average of 9.1% and 32.1% with the dc-link voltage reconstruction method and the proposed method, respectively. The amplitude of the motor current harmonic at $\lvert 6\omega_g - \omega_e \rvert$ is decreased by an average of 28.1% and 68.8% with the dc-link voltage reconstruction method and the proposed method, respectively.

V. CONCLUSION

This article has proposed an adaptive beat suppression strategy based on voltage angle harmonics regulation for electrolytic capacitorless PMSM drives, which improves the beat suppression effect in FW region. According to the impedance model of FW control, the limitations of the dc-link voltage reconstruction beat suppression method in the FW region are clarified. By establishing a closed loop control between dc-link voltage and voltage angle, the FWC-A is effectively suppressed. The control parameters are adaptively adjusted according to the impedance relationship between the voltage angle and the dc-link voltage to minimize the beat envelope. Compared with the traditional method, the beat suppression ability of the proposed method is further improved, and it has better adaptability to the operating conditions and parameter changes of the motor. Experimental

results show that the beat suppression effect of the proposed method is further increased by more than 50% compared with the conventional method.

REFERENCES

[1] Y. Li, Z. Yin, D. Yuan, Y. Zhang, Y. Gao, and H. Yang, "A Multi-Harmonics suppression backstepping extended state observer for the pmsm electrolytic capacitorless drives sensorless control," *IEEE Trans. Power Electron.*, vol. 40, no. 8, pp. 10769–10782, Aug. 2025 doi: 10.1109/TPEL.2025.3556854.

[2] Y. Sun, Z. Wang, and S. You, "Charging strategy of electrolytic capacitorless integrated OBC for electric vehicles with high-frequency voltage pulses in intermediate link," *IEEE Trans. Power Electron.*, vol. 40, no. 7, pp. 9737–9748, Jul. 2025.

[3] Y. Wang, H. Cao, I. Colak, Y. Zhang, and J. Shen, "Experimental study on characteristics variation of permanent magnets for high-speed machine applications," *Chin. J. Elect. Eng.*, vol. 8, no. 1, pp. 16–23, Mar. 2022.

[4] J. Liu and Y. Zhang, "DC-link voltage stabilization based on complex-coefficient current controller for IPMSM drives without electrolytic capacitors," *IEEE Trans. Ind. Electron.*, vol. 72, no. 4, pp. 3346–3356, Apr. 2025.

[5] D. Wen, W. Wang, and Y. Zhang, "Sensorless control of permanent magnet synchronous motor in full speed range," *Chin. J. Elect. Eng*, vol. 8, no. 2, pp. 97–107, Jun. 2022.

[6] A. V. Deshmukh, M. Afshar, S. Jena, A. M. Hava, Z. Yu, and B. Akin, "A practical control method for single-phase input PMSM drives with small DC-link capacitor," *IEEE Trans. Power Electron.*, vol. 40, no. 3, pp. 4358–4373, Mar. 2025.

[7] R. Antonello, S. Rigon, F. Tinazzi, and M. Zigliotto, "Capacitorless synchronous reluctance motor drives for pump applications with resonance damping and line current harmonics reduction," *IEEE J. Emerg. Sel. Topics Power Electron.*, vol. 11, no. 5, pp. 5279–5289, Oct. 2023.

[8] J. Xiong, J. Zhang, X. Huang, and F. Deng, "Current ripple suppression of PMSM drives under reduced DC-link capacitance considering digital delay," *IEEE J. Emerg. Sel. Topics Power Electron.*, vol. 12, no. 4, pp. 3688–3698, Aug. 2024.

[9] H. Shin, Y. Son, and J.-I. Ha, "Grid current shaping method with dc-link shunt compensator for three-phase diode rectifier-fed motor drive system," *IEEE Trans. Power Electron.*, vol. 32, no. 2, pp. 1279–1288, Feb. 2017.

[10] D. Ding et al., "Impedance reshaping for inherent harmonics in PMSM drives with small DC-link capacitor," *IEEE Trans. Power Electron.*, vol. 37, no. 12, pp. 14265–14279, Dec. 2022.

[11] Z. Re et al., "Adaptive virtual admittance reshaping-based resonance suppression strategy for PMSM drives with small DC-link capacitor," *IEEE Trans. Power Electron.*, vol. 39, no. 3, pp. 3109–3121, Mar. 2024.

[12] L. Mathe, L. Török, D. Wang, and D. Sera, "Resonance reduction for AC drives with small capacitance in the DC link," *IEEE Trans. Ind. Appl.*, vol. 53, no. 4, pp. 3814–3820, Jul./Aug. 2017.

[13] R. Gao, D. Ding, G. Wang, Q. Wang, G. Zhang, and D. Xu, "Feature extraction of frequency-mapping-based resonance suppression in PMSM drives with low DC-link capacitance and inductance," *IEEE Trans. Power Electron.*, vol. 40, no. 4, pp. 4848–4861, Apr. 2025.

[14] W. E. Sayedl, H. Loschi, A. Madi, N. Moonen, R. Smolenski, and F. Leferink, "Low-frequency envelope of DC/DC converters due differences in the control hardware features," in *Proc. Asia-Pacific Int. Symp. Electromagn. Compat.*, Bali, Indonesia, 2021, pp. 1–4.

[15] D. Wang and K. Lu, "Analysis of system interharmonics of VSI-fed small DC-link drive with varying power load," in *Proc. IEEE Energy Convers. Congr. Expo.*, Portland, OR, USA, 2018, pp. 3347–3354.

[16] H. Li, K. Zhang, H. Zhao, S. Fan, and J. Xiong, "Active power decoupling for high-power single-phase PWM rectifiers," *IEEE Trans. Power Electron.*, vol. 28, no. 3, pp. 1308–1319, Mar. 2013.

[17] C. Zhang, R. Gao, X. Zhu, L. Xu, and Y. Du, "Boost-based active power decoupling converter with voltage complementary for electrolytic capacitor-less PMSM drive system," *IEEE Trans. Power Electron.*, vol. 39, no. 9, pp. 11493–11503, Sep. 2024.

[18] Y. Ohno and H. Haga, "Control method of electrolytic capacitorless dual inverter for harmonic compensation under distorted grid voltage," *IEEE Trans. Ind. Appl.*, vol. 58, no. 1, pp. 375–387, Jan./Feb. 2022.

[19] H. Ouyang, K. Zhang, P. Zhang, Y. Kang, and J. Xiong, "Repetitive compensation of fluctuating DC Link voltage for railway traction drives," *IEEE Trans. Power Electron.*, vol. 26, no. 8, pp. 2160–2171, Aug. 2011.

[20] D. Ding, N. Zhao, G. Wang, G. Zhang, X. Zhang, and N. Mijatovic, "Suppression of beat phenomenon for electrolytic capacitorless motor drives accounting for sampling delay of DC-link voltage," *IEEE Trans. Ind. Electron.*, vol. 69, no. 2, pp. 1167–1176, Feb. 2022.

[21] Z. Ren et al., "Beat phenomenon suppression method based on repetitive control for reduced DC-link capacitance IPMSM drives," in *Proc. Int. Conf. Elect. Machines Syst.*, Gyeongju, South Korea, 2021, pp. 626–631.

[22] T. Ardriani et al., "A novel method to reduce low-frequency output current ripple of PWM inverters," *IEEE Trans. Ind. Appl.*, vol. 58, no. 5, pp. 6332–6342, Sep./Oct. 2022.

[23] D. Ding et al., "Beatless control strategy based on impedance reshaping for PMSM drives with small DC-link capacitors," *IEEE Trans. Ind. Electron.*, vol. 71, no. 7, pp. 6829–6840, Jul. 2024.

[24] J. Liu and Y. Zhang, "Current pulsation suppression method based on power current closed-loop control for a PMSM under fluctuating DC-link voltage," *IEEE Trans. Power Electron.*, vol. 37, no. 1, pp. 761–770, Jan. 2022.

[25] N. Zhao, G. Wang, B. Li, R. Zhang, and D. Xu, "Beat phenomenon suppression for reduced DC-link capacitance IPMSM drives with fluctuated load torque," *IEEE Trans. Ind. Electron.*, vol. 66, no. 11, pp. 8334–8344, Nov. 2019.

[26] R. Gao, D. Ding, G. Wang, Q. Wang, G. Zhang, and D. Xu, "Linear modulation region expansion strategy based on voltage vector angle regulation for PMSM drives with small DC-link capacitor," *IEEE Trans. Power Electron.*, vol. 38, no. 7, pp. 8327–8339, Jul. 2023.

[27] D. Ding et al., "Adaptive modulation index fluctuation suppression strategy for electrolytic capacitorless PMSM drives," *IEEE Trans. Transport. Electrific.*, vol. 11, no. 2, pp. 6406–6417, Apr. 2025.

[28] D. Stojan, D. Drevensek, Ž. Plantic, B. Grcar, and G. Stumberger, "Novel field-weakening control scheme for permanent-magnet synchronous machines based on voltage angle control," *IEEE Trans. Ind. Appl.*, vol. 48, no. 6, pp. 2390–2401, Nov./Dec. 2012.

Tianqi Zhang received the B.S. degree in electrical engineering in 2023 from the Harbin Institute of Technology, Harbin, China, where he is currently working toward the M.S. degree in power electronics and electrical drives.

His current research interest includes advanced control strategies for electrolytic capacitor-less drives.

Dawei Ding (Member, IEEE) received the B.S. and M.S. degrees in electrical engineering from Hefei University of Technology, Hefei, China, in 2014 and 2017, respectively, and the Ph.D. degree in electrical engineering from Harbin Institute of Technology (HIT), Harbin, China, in 2021.

He is currently an Associate Professor with the School of Electrical Engineering and Automation, HIT. From 2020 to 2021, he was a Visiting Ph.D. Student with Technical University of Denmark. He has authored more than 50 journal papers in IEEE Transactions and held tens of authorized Chinese invention patents. His current research interests include advanced control of permanent magnet synchronous motor drives and electrolytic capacitorless ac motor drives.

Gaolin Wang (Senior Member, IEEE) received the B.S., M.S., and Ph.D. degrees in electrical engineering from Harbin Institute of Technology, Harbin, China, in 2002, 2004, and 2008, respectively.

In 2009, he was with the Department of Electrical Engineering, Harbin Institute of Technology as a Lecturer, where he has been a Full Professor of Electrical Engineering since 2014. From 2009 to 2012, he was a Postdoctoral Fellow with Shanghai Step Electric Corporation. He has authored more than 70 technical papers published in IEEE Transactions. He is the Holder of 40 Chinese patents. His current major research interests include permanent magnet synchronous motor drives and power converters.

Dr. Wang is a Guest Associate Editor for IEEE TRANSACTIONS ON INDUSTRIAL ELECTRONICS, an Associate Editor for IEEE TRANSACTIONS ON TRANSPORTATION ELECTRIFICATION, and *IET Electric Power Applications*.

Yihua Hu (Senior Member, IEEE) received the B.S. degree in electrical engineering and the Ph.D. degree in power electronics and drives from China University of Mining and Technology, Xuzhou, China, in 2003 and 2011, respectively.

Between 2011 and 2013, he was with the College of Electrical Engineering, Zhejiang University as a Postdoctoral Fellow. Between 2013 and 2015, he was a Research Associate with the Power Electronics and Motor Drive Group, University of Strathclyde. Between 2016 and 2019, he was a Lecturer with the Department of Electrical Engineering and Electronics, University of Liverpool. Between 2019 and 2023, he was a Reader and electrical engineering group head with the Department of Electronics Engineering, University of York. He is currently a Reader with King's College London. He has authored and coauthored more than 250 papers in IEEE Transactions journals. His research interests include renewable generation, power electronics converters and control, electric vehicle, more electric ship/aircraft, smart energy system, and nondestructive test technology.

Dr. Hu is the Associate Editor with IEEE TRANSACTIONS ON INDUSTRIAL ELECTRONICS, *IET Renewable Power Generation*, *IET Intelligent Transport Systems,* and *Power Electronics and Drives*. He is a Fellow of Institution of Engineering and Technology and a Member of U.K. Young Academy. He was awarded Royal Society Industry Fellowship.

Guoqiang Zhang (Senior Member, IEEE) received the B.S. degree from Harbin Engineering University, Harbin, China, in 2011, and the M.S. and Ph.D. degrees from Harbin Institute of Technology (HIT), Harbin, China, in 2013 and 2017, respectively, all in electrical engineering.

Since 2017, he has been a Faculty Member with the School of Electrical Engineering and Automation, HIT, where he is currently a Professor.

Dianguo Xu (Fellow, IEEE) received the B.S. degree in control engineering from Harbin Engineering University, Harbin, China, in 1982, and the M.S. and Ph.D. degrees in electrical engineering from Harbin Institute of Technology (HIT), Harbin, China, in 1984 and 1989, respectively.

In 1984, he was with the Department of Electrical Engineering, HIT as an Assistant Professor. Since 1994, he has been a Professor with the Department of Electrical Engineering, HIT. He was the Dean of School of Electrical Engineering and Automation, HIT from 2000 to 2010. He was the Vice President of HIT from 2014 to 2020. He authored and coauthored more than 600 technical papers. His research interests include renewable energy generation technology, power quality mitigation, sensorless vector controlled motor drives, high performance servo system.

Dr. Xu is a Chair of IEEE Harbin Section, Co-EIC of IEEE TRANSACTIONS ON POWER ELECTRONICS, Associate Editor for IEEE TRANSACTIONS ON INDUSTRIAL ELECTRONICS and IEEE JOURNAL OF EMERGING AND SELECTED TOPICS IN POWER ELECTRON.